# ESMO Research Research Fellowship
(September 2018– August 2019)


## Michael-John Devlin


### FINAL REPORT


Host Institute: **Barts Cancer Institute**
Mentor: Professor Frances Balkwill
Project title: The immune microenvironment of a murine model of clear cell ovarian cancer

Home Institute: **University College London**


***Introduction***

Clear cell ovarian cancer (CCOC) accounts for 3.4% of ovarian cancers in Europe, a figure which has largely remained stable over time. The incidence is increasing in Asia, where it accounts for around 27% of ovarian cancers in Japan[1-4]. CCOC is resistant to chemotherapy and as such, patients with advanced stage disease have a poor prognosis[5-7].

Some patients who have received treatment with drugs which target the programmed cell death protein 1 (PD1) checkpoint have had complete or partial responses, however not all patients respond and not all responses are durable[8-11]. To understand the mechanism of both response and resistance we need to understand the tumour microenvironment de novo however little information exists in the literature.

ARID1A (the AT-rich interaction domain 1A, BAF250a) is a subunit of the SWItch/Sucrose Non-Fermentable (SWI/SNF) chromatin remodelling complex[12] and is mutated in up to 57% of CCOC[13-14]. ARID1A facilitates the interaction between chromatin and the mismatch repair (MMR) protein MSH2 during DNA replication and repair; in preclinical studies a loss of ARID1A resulted in the inability of MSH2 to perform its function[15] resulting in an MMR phenotype. In a pre-clinical study, knock-out of ARID1A lead to an upregulation of PDL1[16]. Additionally, two other pre-clinical studies suggested that loss of ARID1A function increases IL-6 production however a retrospective study of 192 patients with early stage CCOC, there was no association between ARID1A status and IL-6 production[17-19]. Whether ARID1A impacts on the TME of human CCOC is unknown.

***Rationale and Aim***

1. Undertake a quantitative, qualitative and topographical analysis of the TME of advanced CCOC
2. Determine the impact of an ARID1A mutation on the TME of advanced CCOC
3. Use this information to validate a recently developed model of disease for use as a translational tool

***Experimental design***

1. FFPE samples from 45 cases of CCOC were analyzed; 9 were FIGO I-II and 36 were FIGO III-IV. Immunohistochemistry was performed for; T cells (CD3, CD8, CD45RO, CD4, FOXP3), macrophages (CD68, CD163), B cells (CD20, CD138), mast cells (mast cell

tryptase), dendritic cells (CD1A, LAMP3), eosinophils, fibroblasts (αSMA), neutrophils (CD66b), PD1, PDL1, PDL2 and versican. Collagen was identified using Massons Trichrome and quantified in regard to its structure and texture.

2. I analyzed how each of these populations and metrics varied across the TME by quantifying regions within the malignant cell area (MCA), leading edge (LE) and stroma in paired samples. I then looked at the positive and negative correlations between the metrics within each of these regions.

3. I interrogated RNA sequencing data from a set of 14 early- and 11 late-stage CCOC

4. I constructed multicellular models of disease using eight cell lines (ES-2, TOV-21G, RMG1, OVMANA, OVISE, OVAS, KOC7C, OVTOKO) cultured with immune cells within a collagen gel.

***Results, Conclusions and Future Perspectives***

**1. Results**

***I. Deconstruction of advanced stage CCOC***

- With the exception of LAMP3+ dendritic cells, all immune cells profiled were present throughout the MCA, LE and stroma and displayed variation in quantity and phenotype between these areas and between patients. Plasma cell concentration was highest within the MCA; anti-CD138 CART cells are currently undergoing evaluation for the treatment of multiple myeloma and may be an interesting therapeutic approach in the treatment of advanced CCOC. ***Figures 1.1 – 1.9***

- The collagen ECM displays regional properties which vary across the MCA, LE and stroma. As we move further from the tumour and into the stroma, there is an increase in collagen area. The fibres within the collagen become longer, thicker and move closer together, overlapping to form a matrix that is diffuse and orientated in many different directions. ***Figures 1.10-1.11***

- The malignant cells were shown to express high levels of PDL2, which was the dominant ligand throughout the TME of advanced CCOC. PDL2 shared a positive association with PD1 at the LE and both shared negative associations with T cells, B cells, macrophages and eosinophils in this region. This suggests that binding of PDL2 to PD1 at the LE also contributes to a pro-tumour immune environment and may offer an explanation as to why anti-PD-1 drugs have demonstrated the ability to generate a complete response in advanced CCOC, whereas drugs targeting PDL1 have only generated a partial response. ***Figure 1.12***

- Collagen thickness is the feature with the most immune cell corelations, the majority of which are negative. Tumours with fibres which are thinner, share an identical immune profile to tumours with a high immunoscore, suggesting this ECM feature is the most important in promoting a pro-tumour immune environment. ***Figure 1.13-1.14***

- The large number of cytotoxic CD8+ cells, their location at the LE and their close proximity to both B cells and memory T cells are all positive prognostic markers for response to

checkpoint inhibition in other malignancies, and suggest that in advanced CCOC the immune system is primed to respond following interruption of the PD1/PDL2 axis. I hypothesise that this response may be augmented by combination therapy with an agent that interferes with collagen metabolism, such as cyclophosphamide, which is already licenced in advanced ovarian cancer and has been shown to reduce collagen deposition in patients with sclerodema.

- When I compared the TME of early versus late stage CCOC, there was no significant difference in the populations of T cells, B cells, mast cells or macrophages, however there were significantly more fibroblasts in the stroma of advanced stage disease. The ECM was significantly different, with advanced stage disease having more collagen, with longer more heterogenous fibres which overlapped to form a diffuse matrix. RNA sequencing analysis found that restructuring of the ECM via TGF-β signalling was one of the most enriched pathways as the disease became advanced. Combinations of anti-PD-1 and anti-TGF-β are currently undergoing clinical assessment for other tumour types and may help increase durable responses in advanced CCOC. ***Figures 1.15-1.20***

### *II. Impact of ARID1A mutation on the TME of advanced CCOC*

- When I compared ARID1A wildtype ($ARID1A^{wt}$) to ARID1A mutant ($ARID1A^{mut}$) tumours, $ARID1A^{wt}$ had more collagen, with longer fibers and more branchpoints across the MCA, LE and Stroma. Within the LE and Stroma of $ARID1A^{wt}$ tumours, collagen fibers formed a more diffuse isotropic matrix. ***Figure 1.21***

- The LE of $ARID1A^{mut}$ was the most immune rich region, with the largest populations of CD45RO T-cells, CD20 B-cells and Mast Cells. The LE of $ARID1A^{wt}$ tumours had the largest populations of CD4 and CD8 T-Cells. There were significantly more CD3 T-cells within the MCA of $ARID1A^{mut}$ tumours and significantly more at the LE and within the stroma of $ARID1A^{wt}$. In $ARID1A^{mut}$ tumours there was significantly more PDL1 expression within the MCA compared to $ARID1A^{wt}$ tumours, which had more PD-1 at the LE and significantly more PDL2 within both the MCA and LE. ***Figures 1.22-1.23***

- My results support pre-clinical findings that that loss of ARID1A leads to upregulation of PDL1 and increased lymphocyte infiltration into the MCA. Both $ARID1A^{wt}$ and $ARID1A^{mut}$ display different features which are associated with response to checkpoint inhibition in other cancers. I suspect the functional status of ARID1A impacts on the pattern and duration of response to checkpoint inhibition and may be a useful biomarker in the future management of CCOC.

### *III. Multicellular Models*

- As the mouse model of CCOC was created using ARID1A knockout, my results from the human disease showed that this would not be a representative tool for all patients with CCOC. I therefore constructed multicellular models of CCOC, using both $ARID1A^{wt}$ and $ARID1A^{mut}$ cell lines.

- I was able to establish a new encapsulated model of disease which replicated the MCA/LE I observed in my deconstruction of the human disease. I have incorporated fibroblasts, monocytes, macrophages, dendritic cells and ongoing work with T cells. ***Figures 1.24-1.26***

- CCOC cell lines have the ability to generate matrix and remodel the ECM on their own, but there is a significantly more diffuse and complex collagen when they are co-cultured with fibroblasts. How the structure of ECM changes with the addition of each successive cell

line is currently ongoing analysis.

**2. Conclusions**

- The TME of advanced CCOC is complex and diverse. The large number of cytotoxic CD8 T cells, their location at the LE, their close proximity to both B cells and memory T cells alongside the high levels of PDL2 expressed on tumour cells suggest that CCOC has an immune microenvironment primed for response after interruption of the PD1 axis.

- Given the associations between collagen thickness and Immunoscore, the combination of a PD1 inhibitor alongside drugs which alter collagen metabolism (such as cyclophosphamide) may increase response rates. Another potential combination would be anti-PD1 with an anti-TGF-β, given that remodelling of the ECM between early and late-stage disease is driven by TGF-β.

- An alternative therapeutic approach may be with anti-CD138 CART cells, given the large population of tumour associated plasma cells in advanced CCOC.

- Loss of ARID1A function significantly alters the TME of advanced CCOC and may impact on the pattern and duration of response. I suspect ARID1A will be a useful biomarker in the future for selecting out patient populations who are more likely to get a durable response from checkpoint inhibition.

- Multicellular models are flexible and representative with the potential to be a powerful translational tool

**3. Future Perspectives**

- I will be involved in the translational analysis of samples from the PEACOCC clinical trial, on which patients with advanced CCOC received treatment with the anti-PD1 drug pembrolizumab. I can use the data generated to date to ensure the translational component is as meaningful as possible.

- I am planning a clinical trial in advanced CCOC that will use checkpoint inhibition in combination with anti-TGF-β or cyclophosphamide. The aim of this study will be to increase response rates to anti-PD1 therapy and to turn non-responders into responders.

- I plan to add further immune cell lineages into the multicellular models, observing how each additional type alters the TME. Eventually, this process will be streamlined to provide a personalized tool for patients at time of diagnosis to help guide treatment decisions.

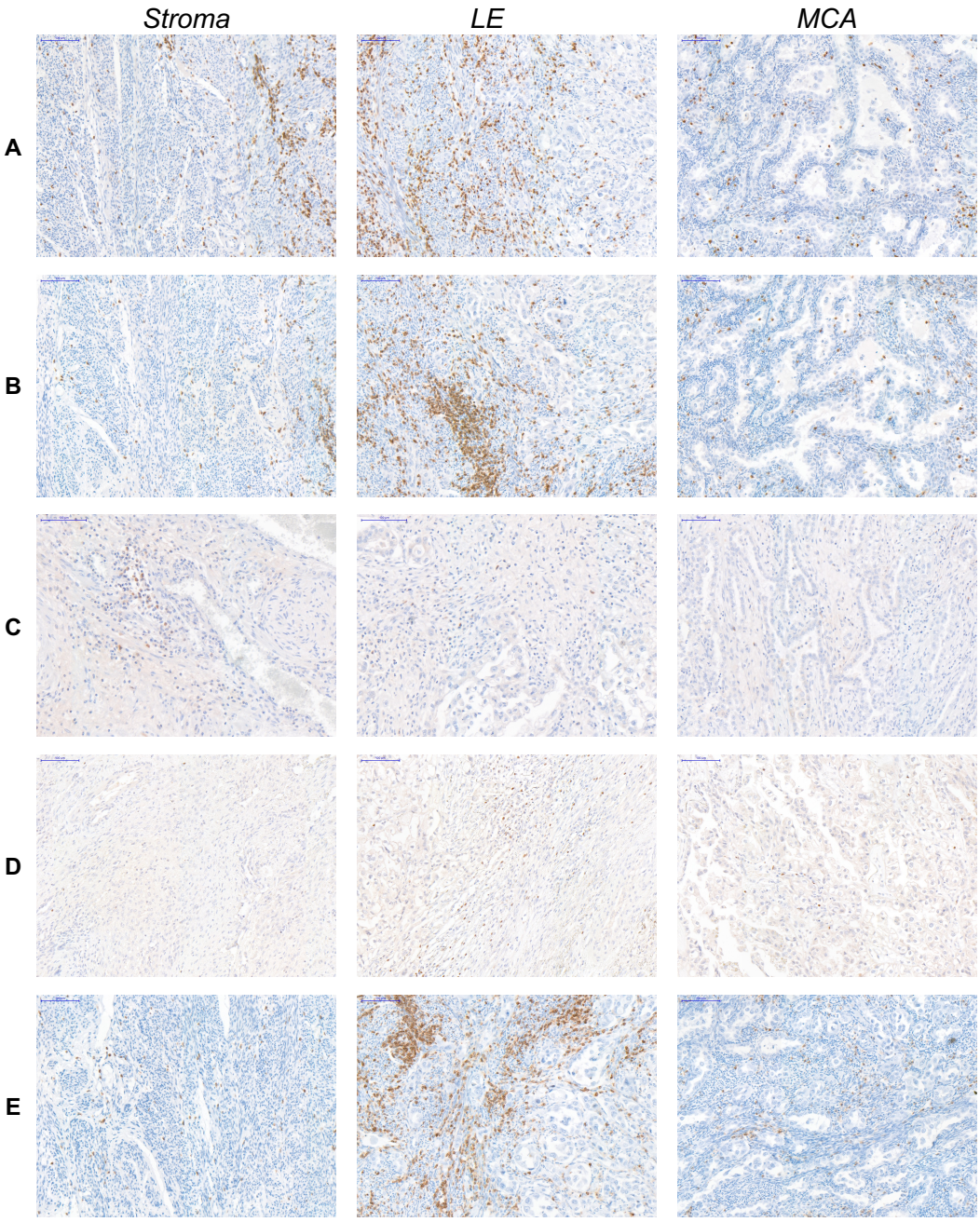


***Figure 1.1 Immunohistochemical identification of T cell subsets across the stroma, leading edge and malignant cell area of advanced clear cell ovarian cancer***
T cells were identified using immunohistochemistry and quantified within the malignant cell area (MCA), leading edge (LE) and stroma. A; CD3, B; CD8, C; CD4, D; FOXP3, F; CD45RO. *There were significantly more CD3, CD8, CD4 and CD45RO cells at the LE than any other region, however the difference between FOXP3 at the LE and stroma was not significant. All images taken x 20 magnification.*

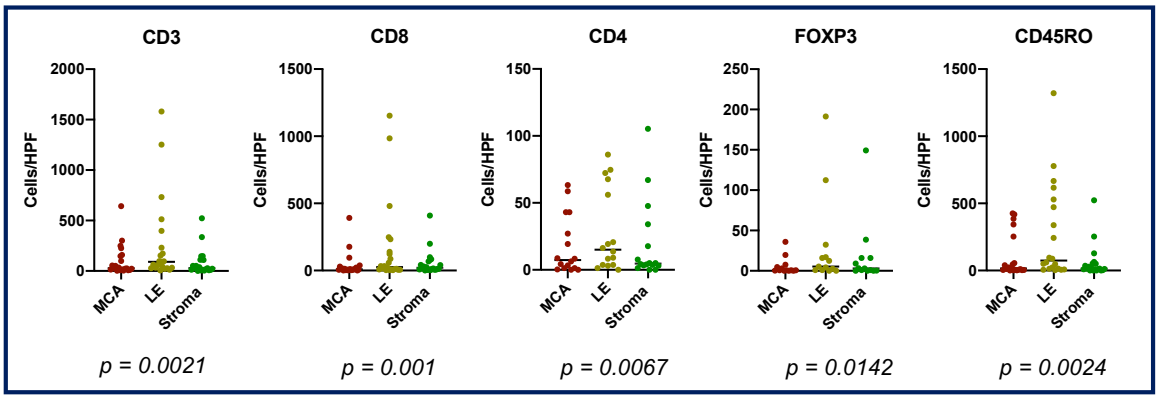


***Figure 1.2 Scatter plots of the average values for T cell markers across the malignant cell area, leading edge and stroma of paired samples***

T cell markers were identified using immunohistochemistry and quantified by cells per high power field (HPF), a HPF being defined as 1x1mm. The distribution of markers across the malignant cell area (MCA), leading edge (LE) and stroma was analyzed in paired samples with significant differences in their distribution throughout the tumour microenvironment identified for all markers.

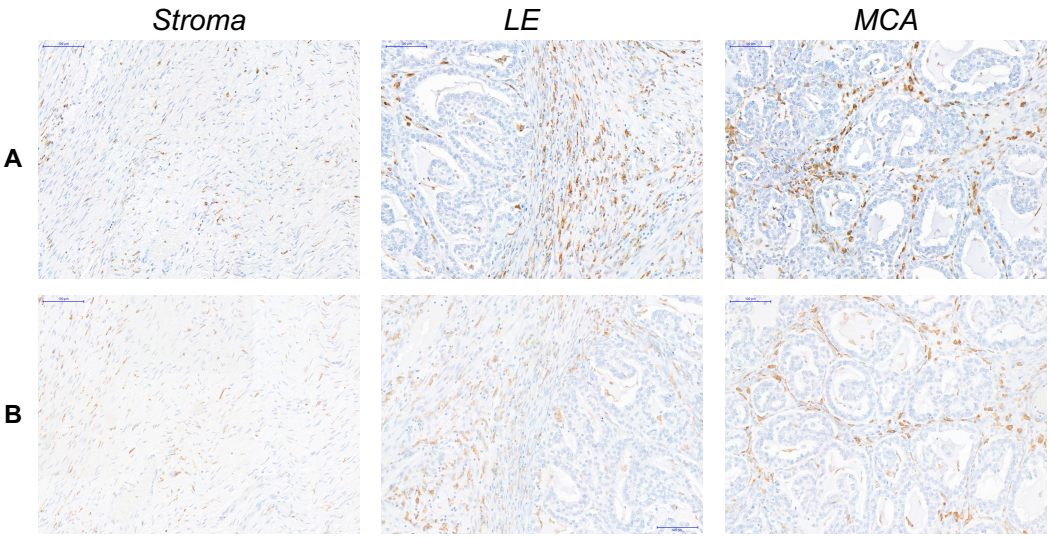


***Figure 1.3 Immunohistochemical identification of macrophage subsets across the stroma, leading edge and malignant cell area of advanced clear cell ovarian cancer***
Macrophages were identified using immunohistochemistry and quantified within the malignant cell area (MCA), leading edge (LE) and stroma. A; CD68, B; CD163. *All images taken x 20 magnification.*

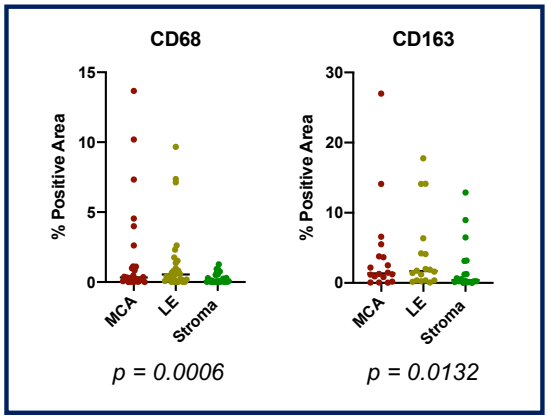


***Figure 1.4 Scatter plots of the average values for macrophage markers across the malignant cell area, leading edge and stroma of paired samples***
Macrophage markers were identified using immunohistochemistry and quantified by percentage positive area. The distribution of markers across the malignant cell area (MCA), leading edge (LE) and stroma was analysed in paired samples with significant differences in their distribution throughout the tumour microenvironment identified for all markers.

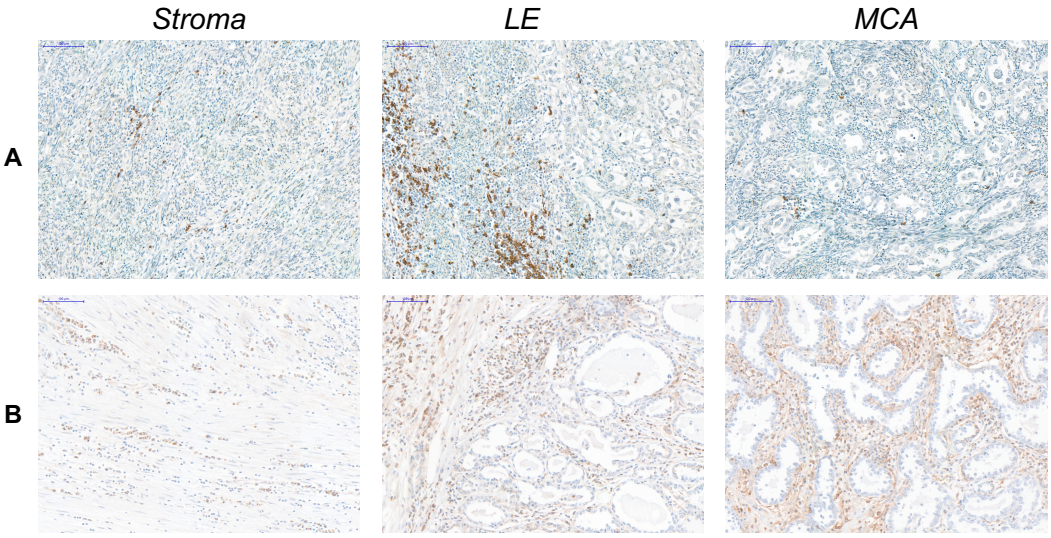


***Figure 1.5 Immunohistochemical identification of B cell subsets across the stroma, leading edge and malignant cell area of advanced clear cell ovarian cancer***
B cells were identified using immunohistochemistry and quantified within the malignant cell area (MCA), leading edge (LE) and stroma. A; CD20, B; CD138. *All images taken x 20 magnification*

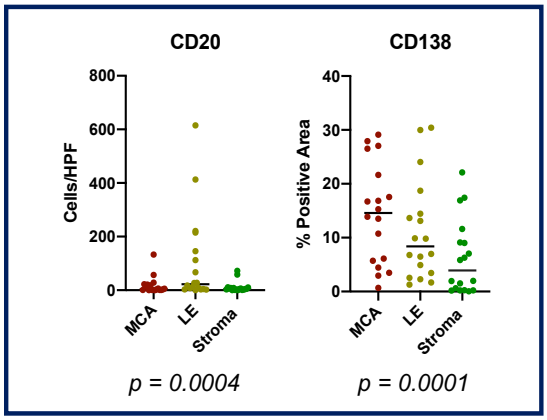


***Figure 1.6 Scatter plots of the average values for B cell markers across the malignant cell area, leading edge and stroma of paired samples***
B cell markers were identified using immunohistochemistry. CD20 was quantified by cells per high power field (HPF), a HPF being defined as 1x1mm. CD138 was quantified by percentage positive area due to the cytoplasmic nature of its staining. The distribution of markers across the malignant cell area (MCA), leading edge (LE) and stroma was analysed in paired samples with significant differences in their distribution throughout the tumour microenvironment identified for all markers.

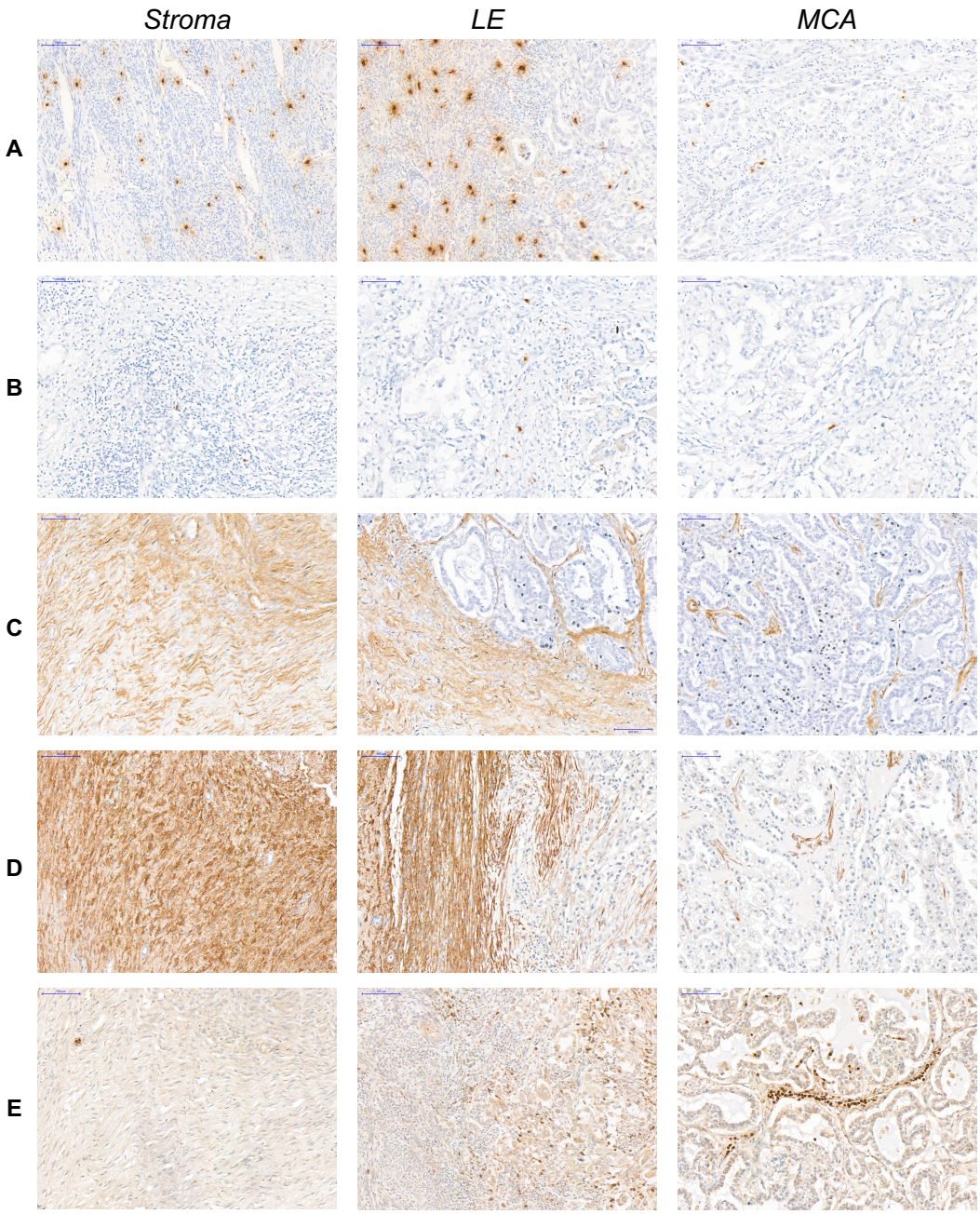


***Figure 1.7 Immunohistochemical identification of immune cell populations across the stroma, leading edge and malignant cell area of advanced clear cell ovarian cancer***
Immune markers were identified using immunohistochemistry and quantified within the malignant cell area (MCA), leading edge (LE) and stroma. A; Mast cell tryptase, B; CD1a, C; αSMA, D; NCAM1, E; CD66b. *All images taken x 20 magnification.*

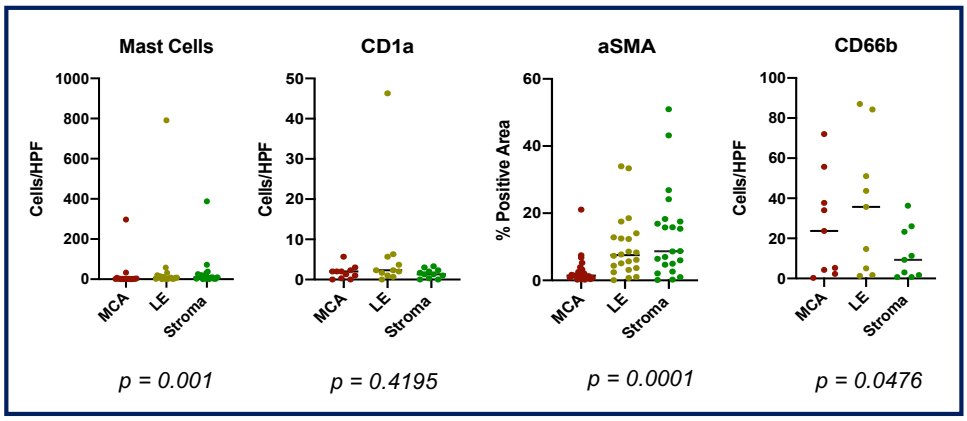


***Figure 1.8 Scatter plots of the average values for immune markers across the malignant cell area, leading edge and stroma of paired samples***
Immune markers were identified using immunohistochemistry and quantified by either cells per high power field (HPF) or percentage positive area. The distribution of markers across the malignant cell area (MCA), leading edge (LE) and stroma was analysed in paired samples which found significant differences in their distribution throughout the tumour microenvironment for all markers except CD1a dendritic cells.

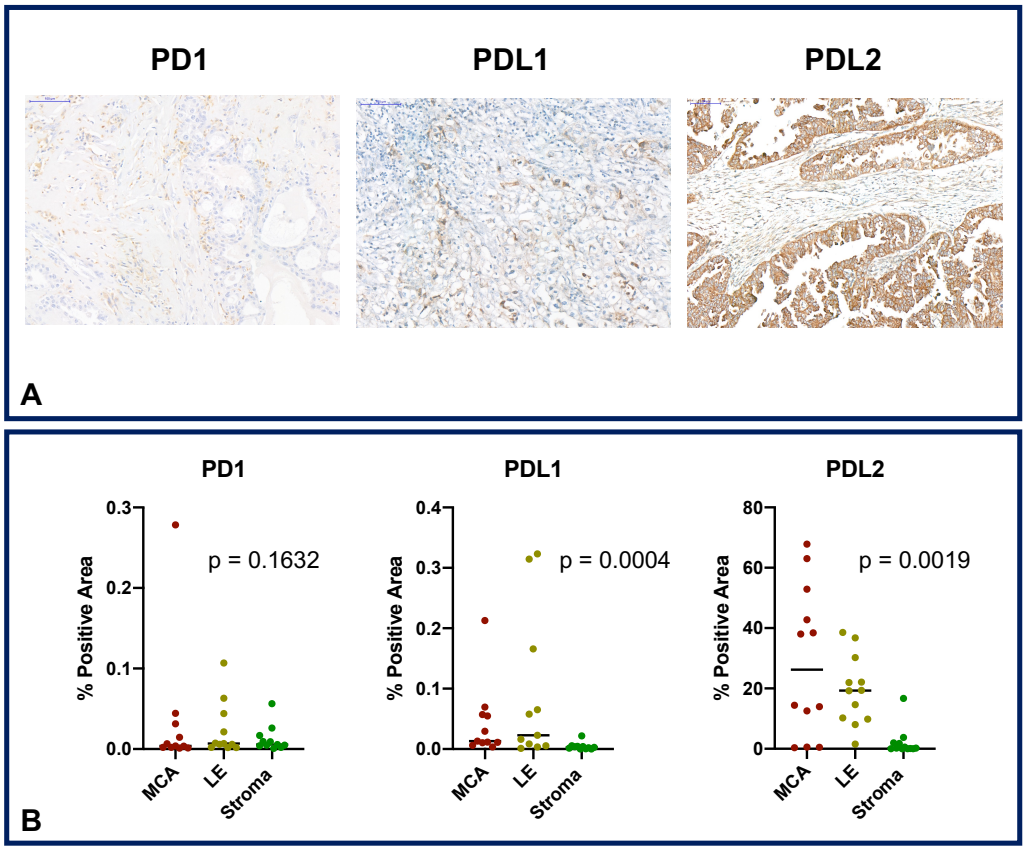


***Figure 1.9 Quantification of PD1 and its ligands, PDL1 and PDL2***
PD1 and its ligands PDL1 and PDL2 were identified by immunohistochemistry, as shown in Figure 4.13A. All checkpoint markers were quantified using positive area and the distribution of markers across the malignant cell area (MCA), leading edge (LE) and stroma was analysed in paired samples as shown in Figure 4.13B. There was no significant difference for PD1 however the was significant variations of both its ligands, with more PD-L1 at the LE and more PDL2 within the MCA.

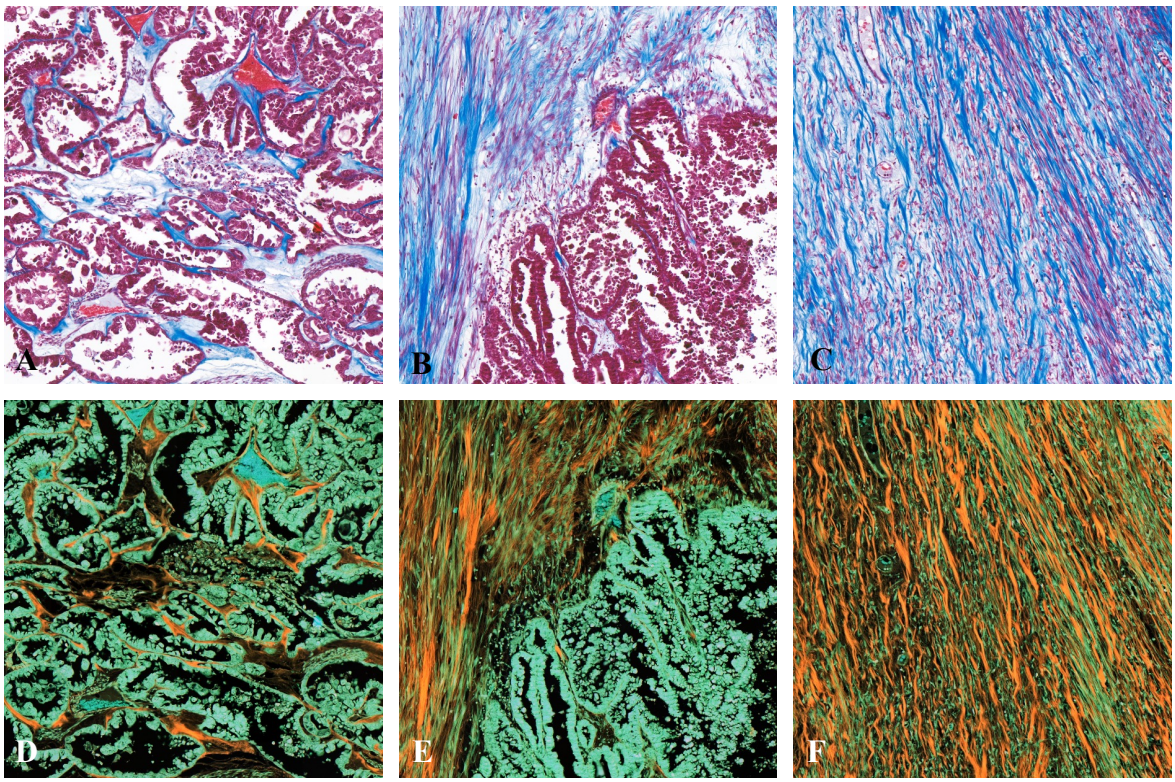


***Figure 1.10 Variation of Masson's Trichrome across the malignant cell area, leading edge and stroma in a sample of advanced clear cell ovarian cancer***
Masson's trichrome was used to identify collagen, shown in blue in the images A-C, which varies across the malignant cell area (A), leading edge (B) and stroma (C). These images were also inverted (D-F) to better visualise the collagen content, shown in orange


***Figure 1.11 Structural and textural properties of collagen across the malignant cell area, leading edge and stroma of advanced clear cell ovarian cancer***
Collagen was identified by Masson's Trichrome and underwent structural and textural analysis. These spider plots show the normalized median values across the malignant cell area, leading edge and stroma. All results are significant at the 0.05 level with the exception of alignment (p=0.8806). *HDM; high density matrix, BCFD; box counting fractal dimension, ASM; angular second moment.*

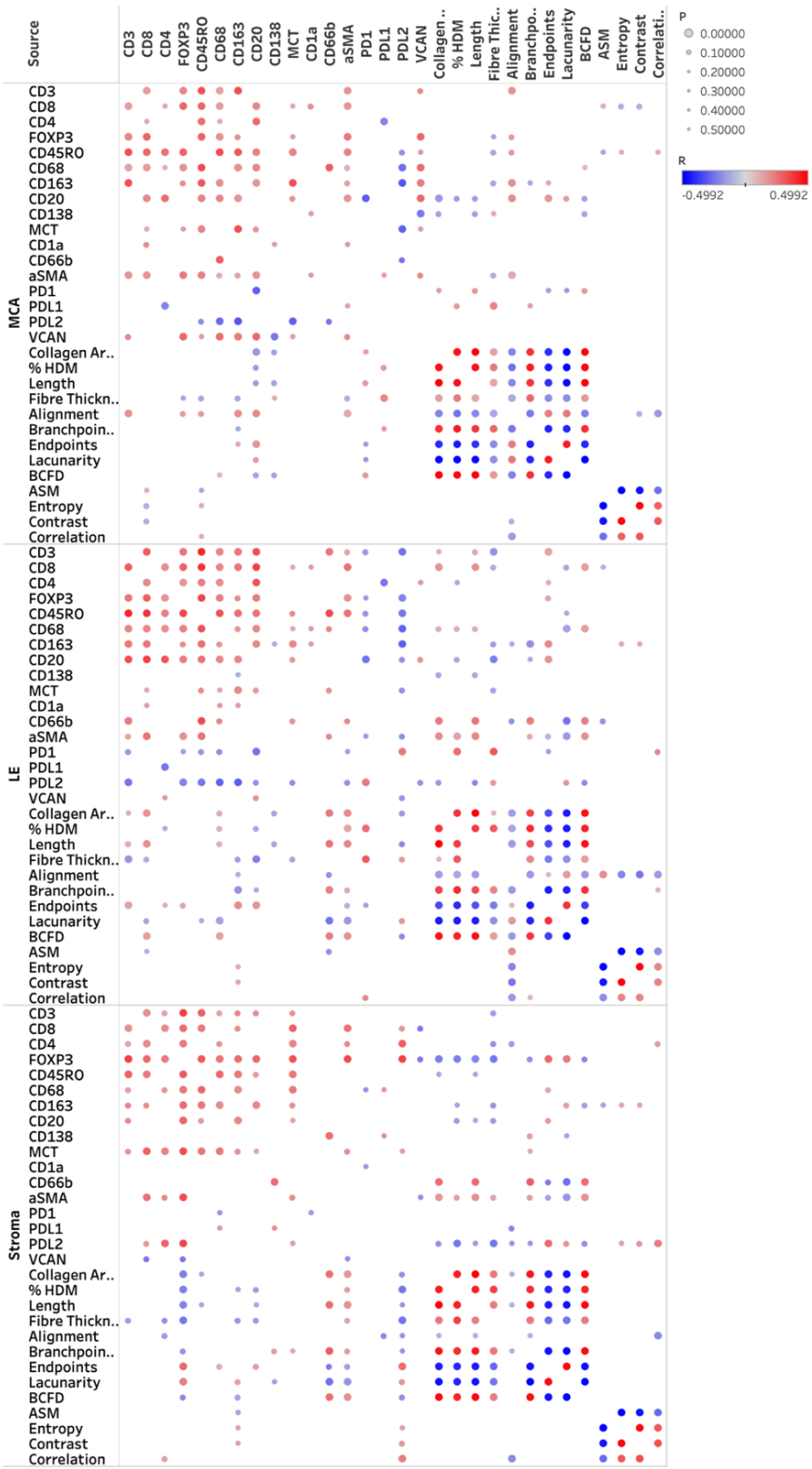


***Figure 1.12*** **Correlations between tumour microenvironment metrics**
The results for the seventeen immune markers and fourteen extracellular matrix metrics across the malignant cell area (MCA), leading edge (LE) and stroma were analysed with correlation coefficient and results significant at 0.05 level plotted. A larger circle represents a more significant value; positive correlations are shown in red and negative in blue.

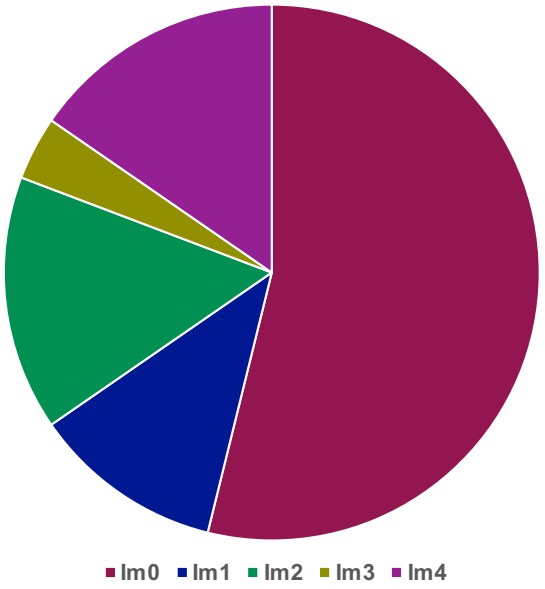


| | Immunoscore | | |
|---|---|---|---|
| | *MCA* | *LE* | *Stroma* |
| CD3 | *** | *** | |
| CD8 | *** | ** | ** |
| MCT | * | | * |
| CD4 | | | |
| FOXP3 | * | | |
| CD20 | * | * | |
| CD45RO | * | * | * |
| CD1a | | | |
| EDN | | | |
| aSMA | * | | |
| PD1 | | * | |
| PDL2 | | ** | |
| PDL1 | | | |
| CD66b | | | |
| CD138 | | | |
| VCAN | * | | |
| CD163 | | | |
| CD68 | | | |
| Area | | | |
| Lacunarity | | | |
| Total Length | | | |
| HGU | | | |
| Branchpoints | | | |
| Endpoints | | | |
| BCFD | | | |
| %HDM | | | |
| Alignment | | | |
| Average Length | | | |
| Fibre Thickness | | * | |
| ASM | | | |
| Contrast | | | |
| Correlation | | | |
| Entropy | | | |

| | |
|---|---|
| | Upregulated with High Immunoscore |
| | Downregulated with High Immunoscore |
| | Insufficient sample size |

| | |
|---|---|
| * | significant at 0.05 level |
| ** | significant at 0.001 level |
| *** | significant at 0.0001 level |

***Figure 1.13 Calculation of Immunoscore for advanced clear cell ovarian cancer***
To calculate the Immunoscore, CD3 and CD8 cells within the malignant cell area and leading edge were quantified and the combined median value across both regions was identified; the individual regions were then subsequently scored as either being above (1) or below (0) this median value and an accumulative score calculated for each sample ranging from 0 (Im0) to 4 (Im4); an overview of the scores for this cohort are shown in the pie chart. A tumour with a value of 3 or 4 was considered to have a high Immunoscore with the significant differences between high and low tumours shown above. Of note a high Immunoscore was associated with less PD1/PDL2 and thinner collagen fibres

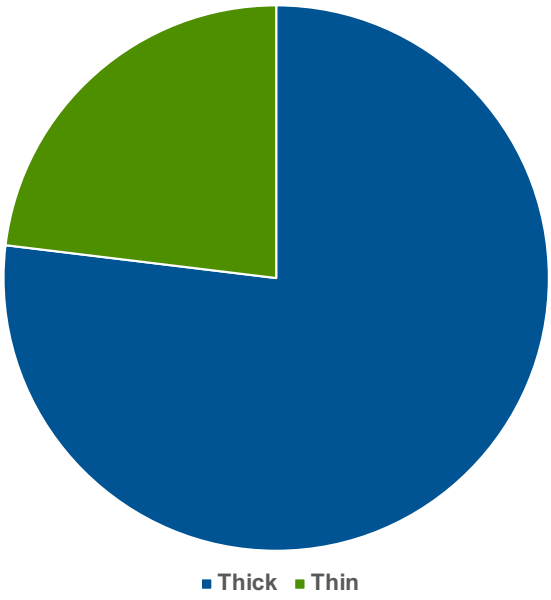


| | Collagen Thickness | | |
|---|---|---|---|
| | *MCA* | *LE* | *Stroma* |
| CD3 | ** | ** | |
| CD8 | ** | ** | * |
| MCT | * | | |
| CD4 | | | |
| FOXP3 | ** | | |
| CD20 | * | * | |
| CD45RO | * | * | * |
| CD1a | | | |
| EDN | | | |
| aSMA | | | |
| PD1 | | * | |
| PDL2 | | * | |
| PDL1 | | | |
| CD66b | | | |
| CD138 | | | |
| VCAN | * | | |
| CD163 | | | |
| CD68 | | | |

| | |
|---|---|
| | Upregulated with Thick Collagen |
| | Downregulated with Thick Collagen |
| | Insufficient sample size |

| | |
|---|---|
| * | significant at 0.05 level |
| ** | significant at 0.001 level |
| *** | significant at 0.0001 level |

***Figure 1.14 Associations between collagen thickness and immune markers at the leading edge in advanced clear cell ovarian cancer***

As collagen thickness at the leading edge (LE) was significantly associated with Immunoscore, I wanted to explore the impact of this metric on immune cell markers. Collagen thickness at the LE was divided into quartiles, and samples within the lowest quartile were classified as having thin collagen while all other patients had thick. Samples within the lowest quartile for thickness share a similar immune profile as those with a high Immunoscore suggesting that this feature may contribute to the phenotypical immune changes quantified by the Immunoscore metric.

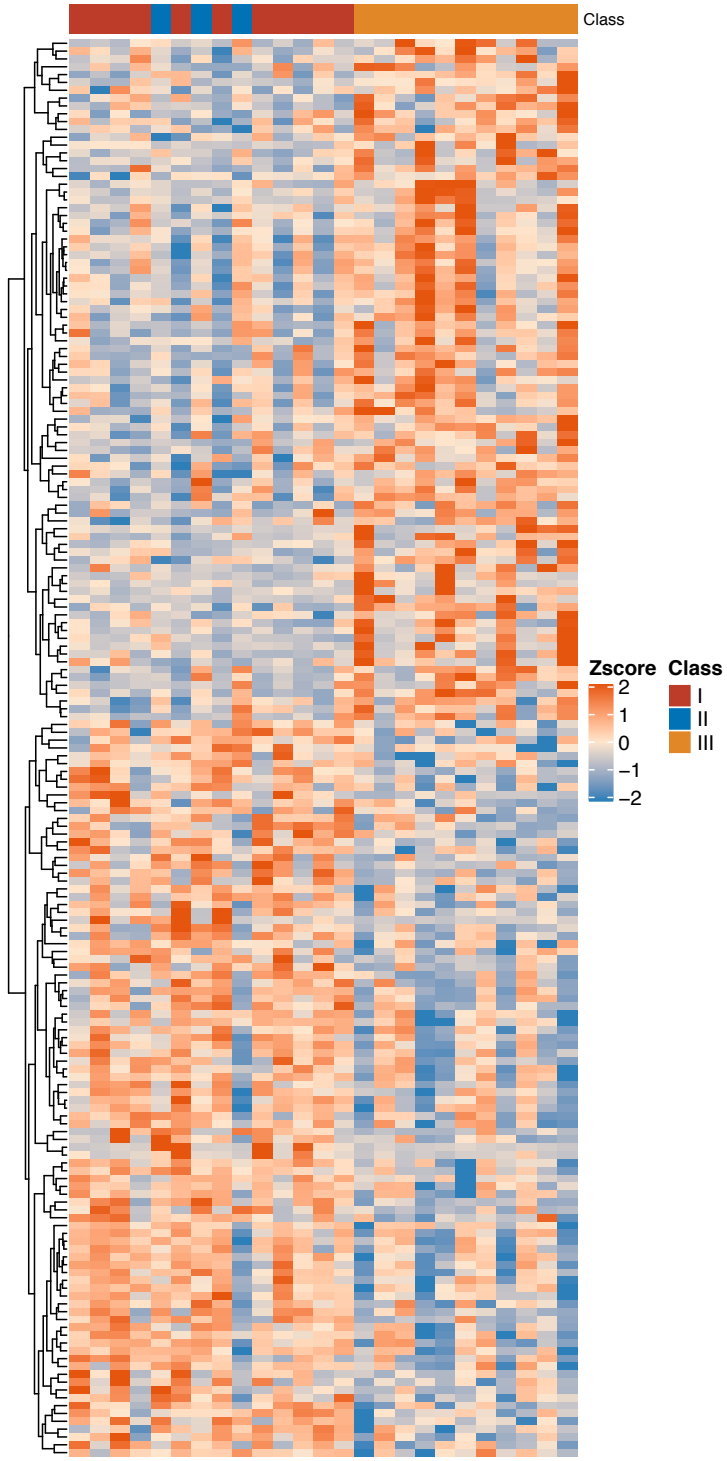


***Figure 1.15 Heatmap showing significantly differentially expressed genes between early and late-stage clear cell ovarian cancer***

A differential expression analysis was performed between early and late stage CCOC, with significance filters applied of p=0.05 and logFC1 which resulted in 181 genes. FIGO stage is displayed along the top, with FIGO I shown as dark red, FIGO II dark blue and FIGO III in orange. Each row represents a differentially expressed gene with upregulated genes shown in red and downregulated in blue.

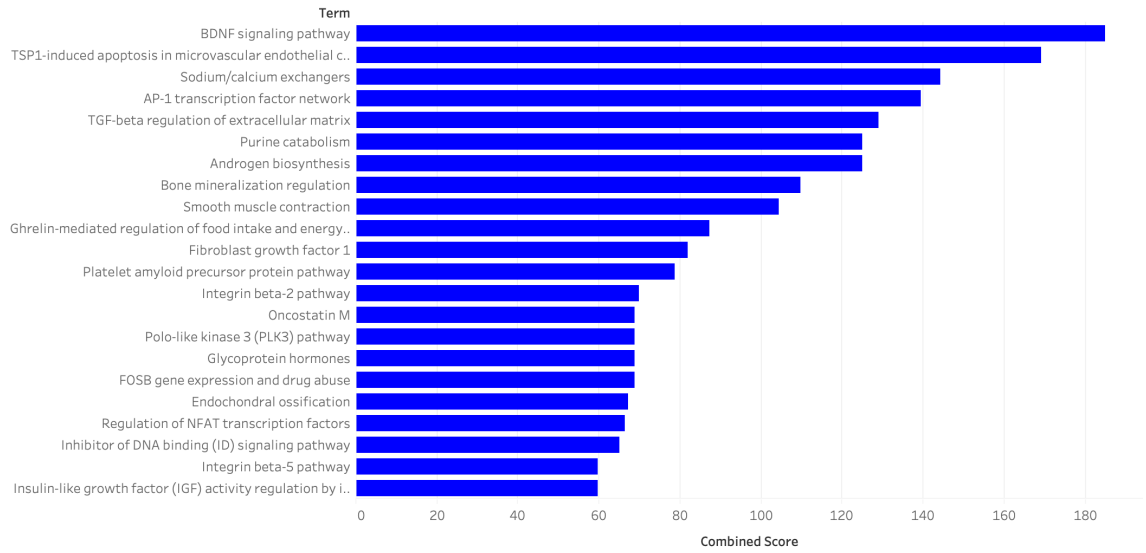


***Figure 1.16*** **BioPlanet pathways which were significantly different between early and late-stage clear cell ovarian cancer.**
The 181 differentially expressed genes from the primary dataset underwent enrichment analysis on the Enrichr platform, with 22 BioPlanet pathways being significantly different with a p value of 0.05 and a combined score >50. The pathways are shown along the vertical axis and the combined score plotted on the horizontal axis, a higher combined score being more significant.

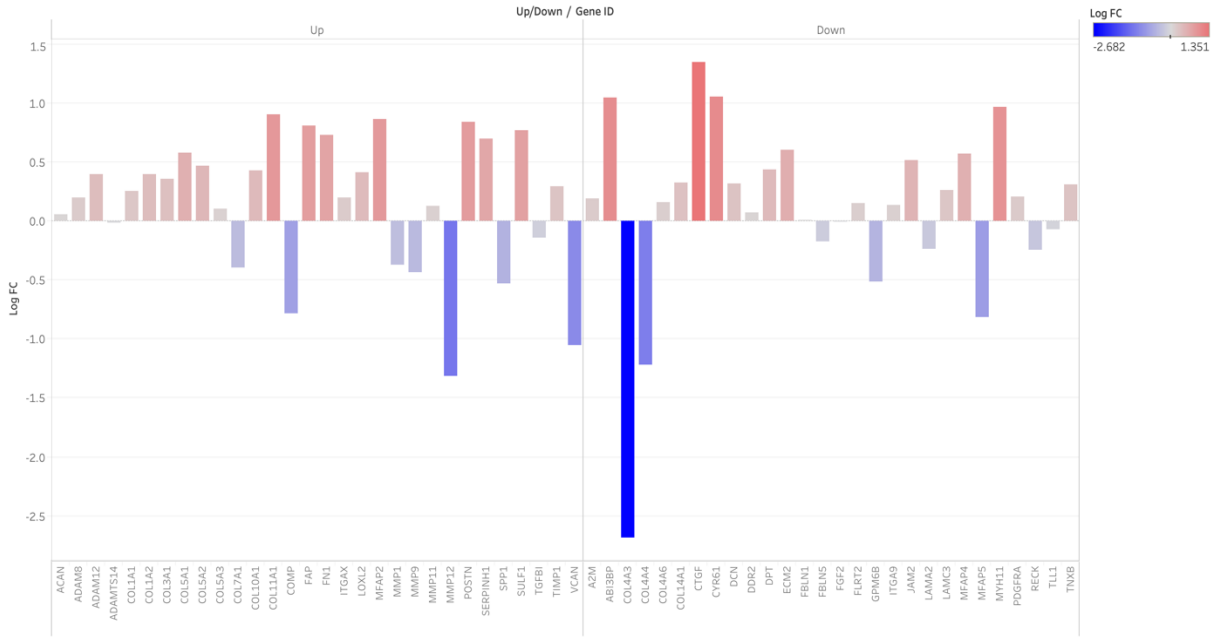


***Figure 1.17 Interrogation of the primary dataset with a TGF-ß cancer-extracellular matrix signature***
The primary dataset was interrogated with a 58 gene signature which is linked to prognosis as well as response to PD-1/PD-L1 checkpoint treatment. This signature consists of 30 upregulated genes which are associated with a poor prognosis and 28 downregulated genes which are associated with a poor prognosis. The signature genes are listed along the bottom of this graph and divided into up (on the left) or down (on the right). The log fold change of each gene, between early- and late-stage disease is plotted, with red showing upregulation in late-stage disease and blue showing downregulation in late-stage disease.

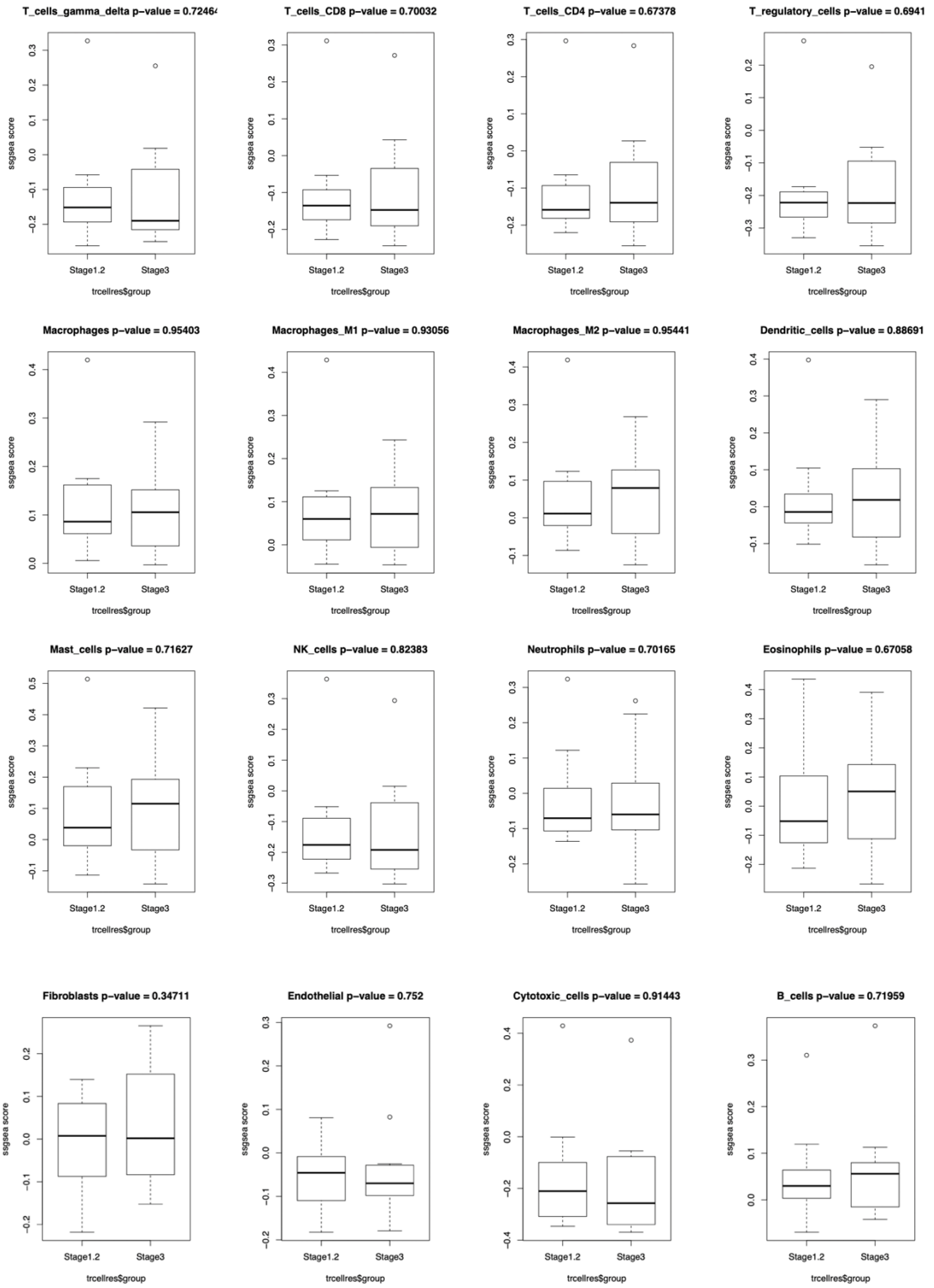


***Figure 1.18*** **CONSENSUS TME cell signatures for the primary dataset**
CONSENSUS TME generates cancer specific signatures for 18 cell types found within the tumour microenvironment. These gene sets are used within a single-sample gene set enrichment analysis (ssGSEA) framework to provide normalized enrichment scores for each of the cell types, representing the relative abundance of cell types across multiple samples. In the primary dataset, CONSENSUS TME showed no significant differences between early- and late-stage CCOC.

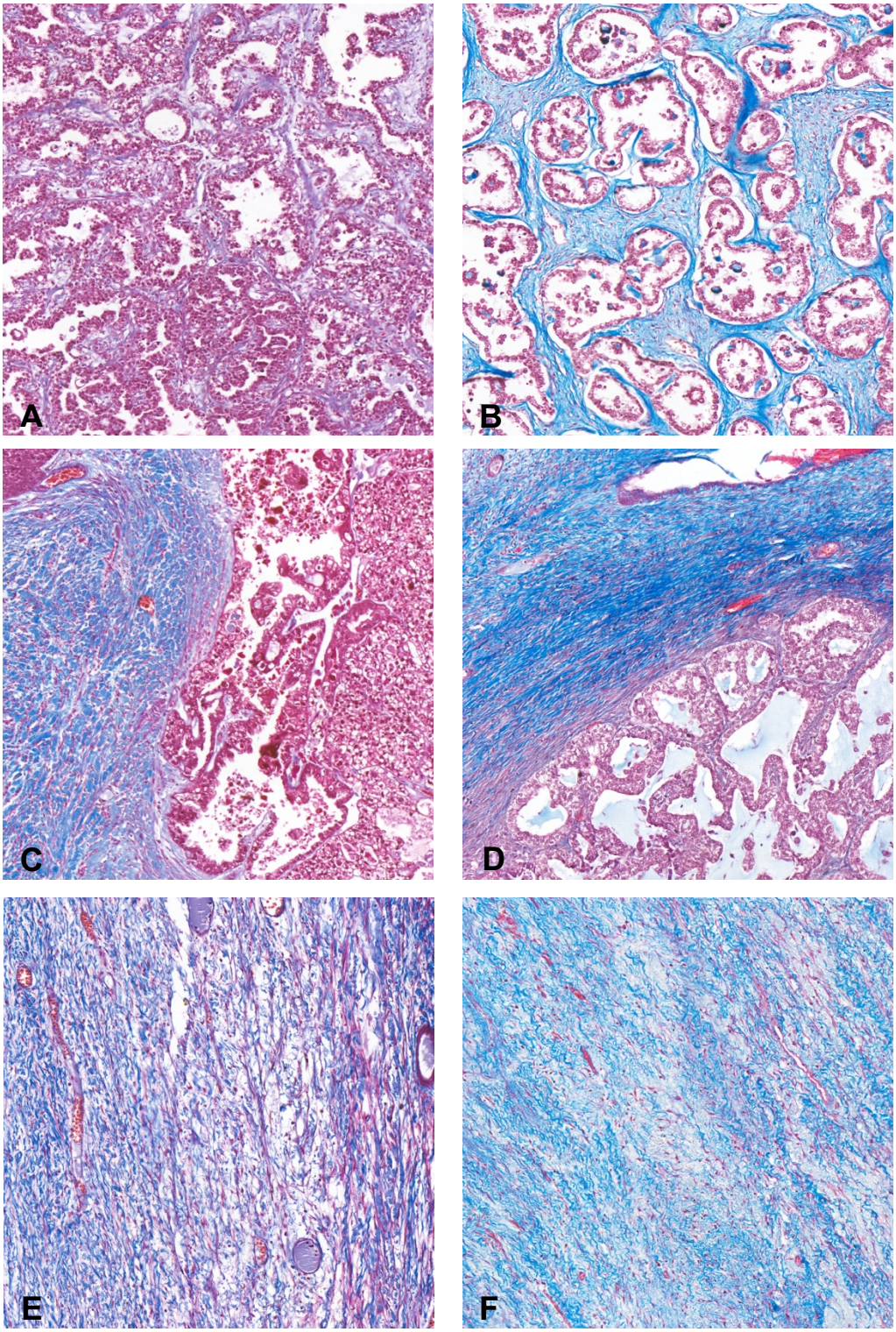


***Figure 1.19*** **Massons Trichrome early of early- and late-stage clear cell ovarian cancer**
Massons Trichrome was used to identify collagen fibres which appears blue in the images above. (A,B) show the malignant cell area, A is early- and B is late-stage. (C,D) show the leading edge, C is early- and D- is late-stage. (E,F) show the stroma, E is early- and F is late-stage CCOC.

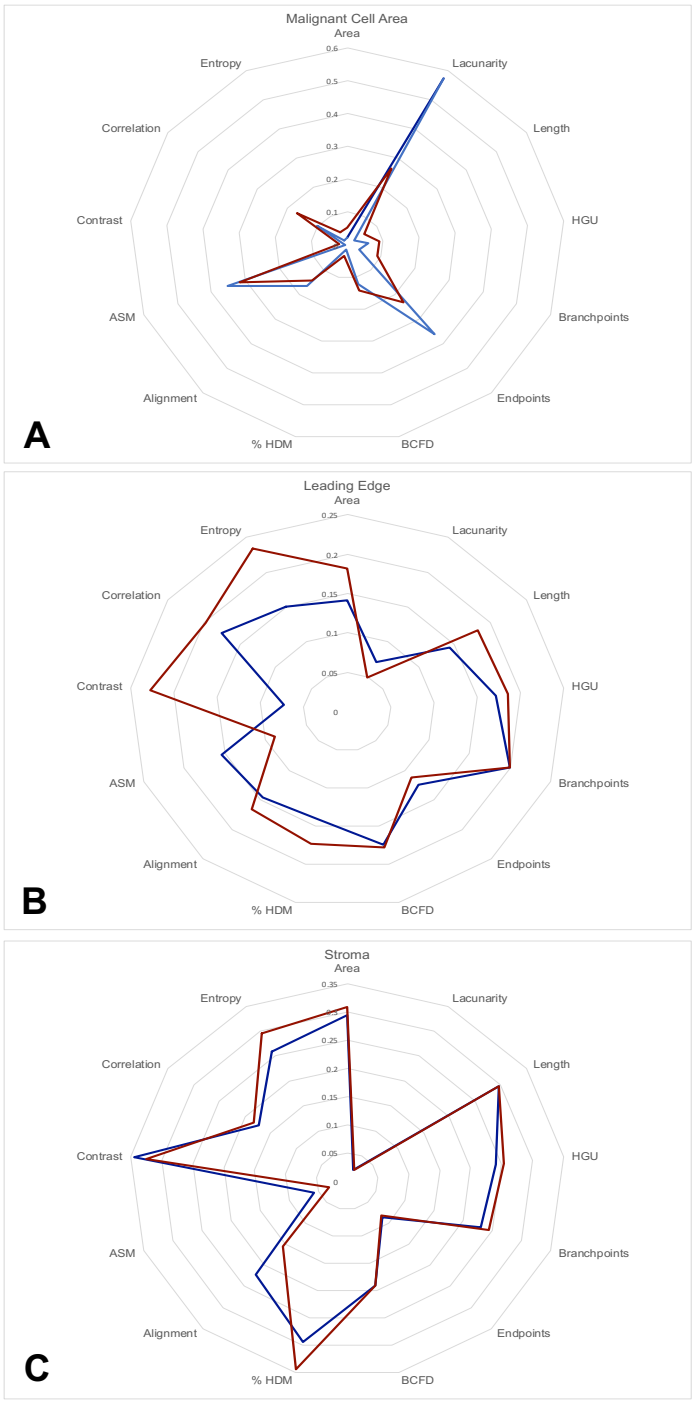


***Figure 1 20*** **Radar Chart of TWOMBLI and Haralick Analysis Features across the malignant cell area, leading edge and stroma of early- and late-stage CCOC.**
Collagen was identified using Massons trichrome and quantified using TWOMBLI and Haralick features, with results normalized to allow comparison between the (A) malignant cell area (B) leading edge and (C) stroma. Red indicates late-stage CCOC and blue is early-stage CCOC. While both share a similar stroma, within the MCA and LE, there is more collagen in late-stage disease with fibres which are longer, closer together and part of a more diffuse matrix.

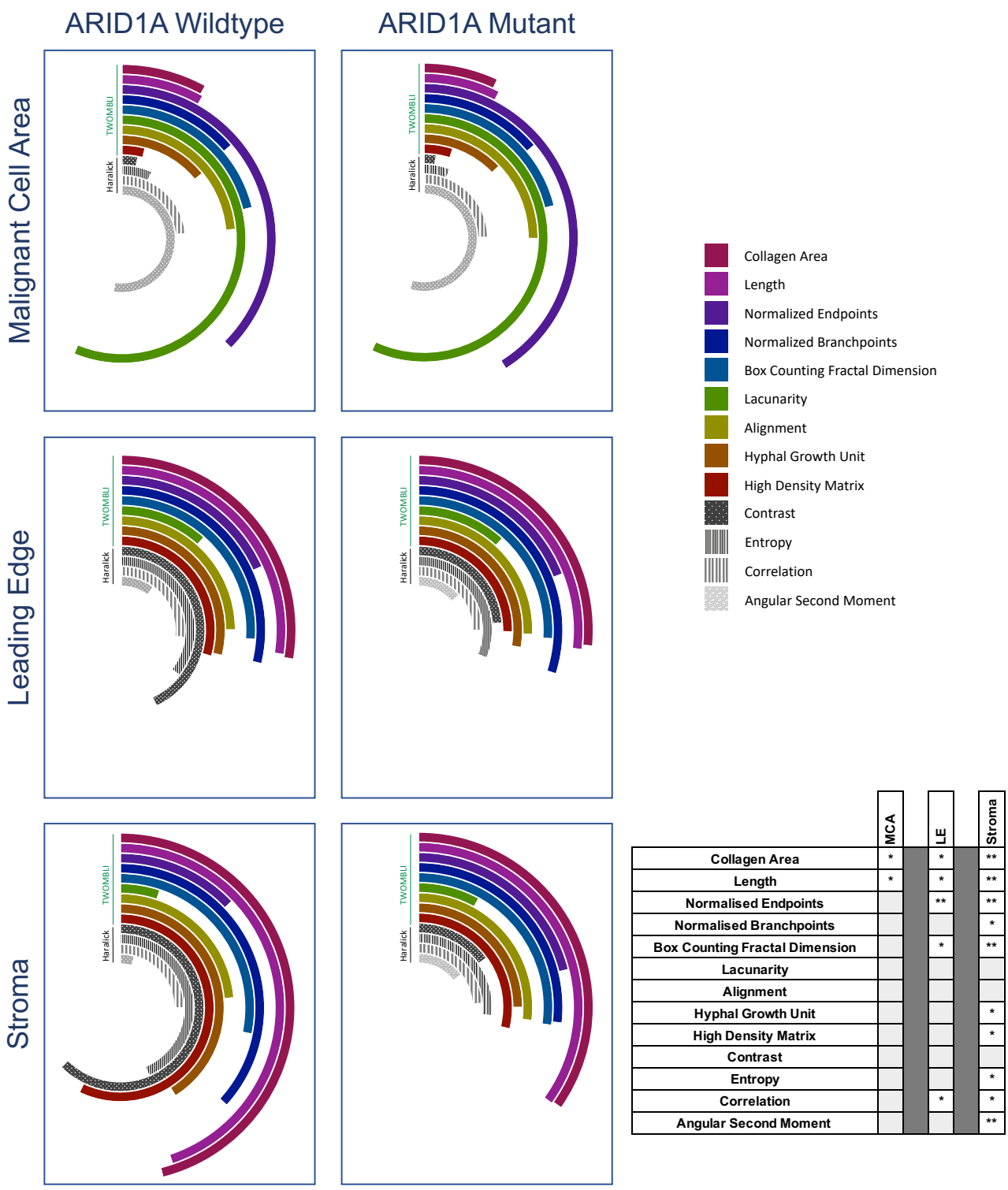


| | MCA | LE | Stroma |
|---|---|---|---|
| Collagen Area | * | * | ** |
| Length | * | * | ** |
| Normalised Endpoints | | ** | ** |
| Normalised Branchpoints | | | * |
| Box Counting Fractal Dimension | | * | ** |
| Lacunarity | | | |
| Alignment | | | |
| Hyphal Growth Unit | | | * |
| High Density Matrix | | | * |
| Contrast | | | |
| Entropy | | | * |
| Correlation | | * | * |
| Angular Second Moment | | | ** |

***Figure 1.21 Radial Bar chart showing the structural and textural changes in collagen between ARID1A wildtype and ARID1A mutant advanced clear cell ovarian cancer***

Collagen was identified by Massons Trichrome and underwent structural and textural analysis. Structural analysis was performed using the FIJI plugin, TWOMBLI, and textural analysis was performed using Haralick features of QuPath V1.2. Across the malignant cell area (MCA), leading edge (LE) and stroma of advanced CCOC, ARID1A wildtype has more collagen with longer fibres compared to ARID1A mutant. Within the LE and stroma, the collagen in ARID1A wildtype tumours are part of a more diffuse matrix.

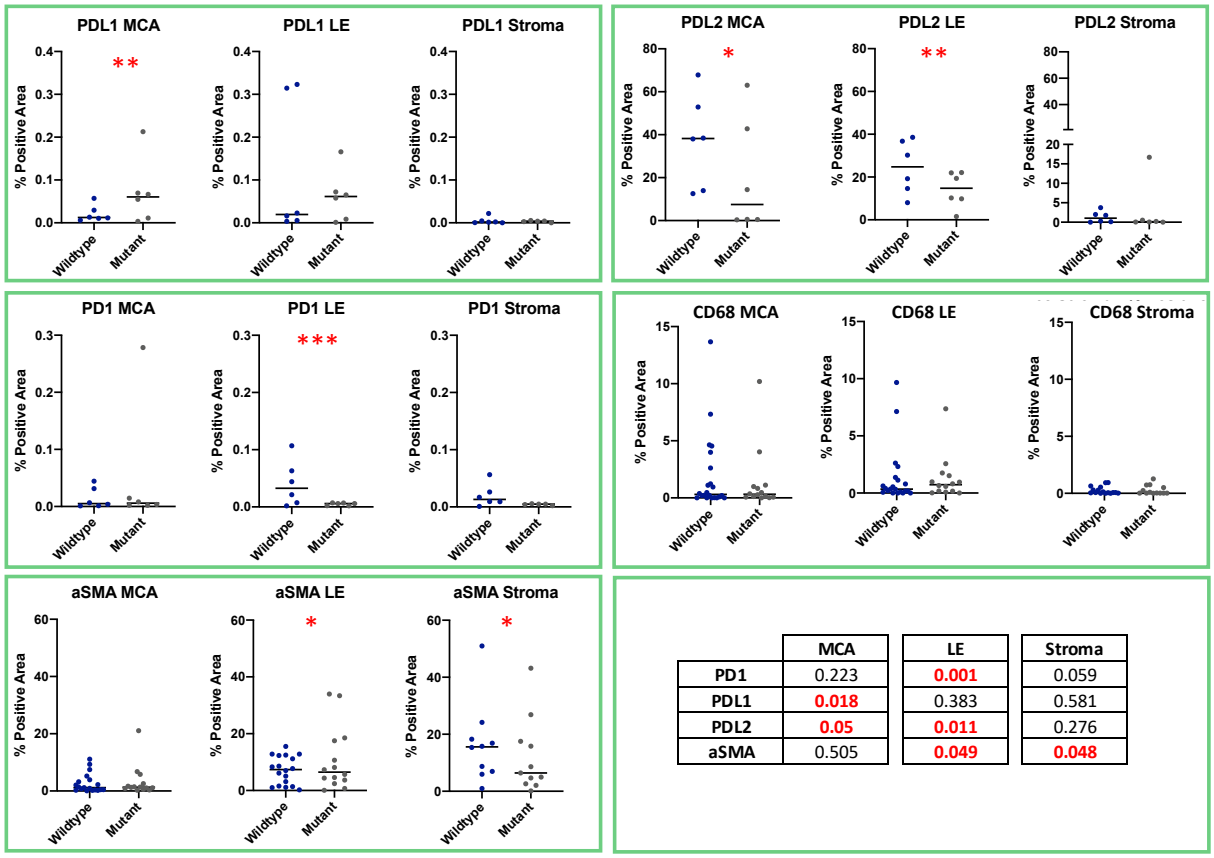


| | MCA | LE | Stroma |
|---|---|---|---|
| PD1 | 0.223 | 0.001 | 0.059 |
| PDL1 | 0.018 | 0.383 | 0.581 |
| PDL2 | 0.05 | 0.011 | 0.276 |
| aSMA | 0.505 | 0.049 | 0.048 |

***Figure 1.23 Variation of immune markers quantified by percentage positive area between ARID1A wildtype and mutant advanced clear cell ovarian cancer***

These scatter plots show the average values for immune markers quantified by positive area across the malignant cell area (MCA), leading edge (LE) and stroma of ARID1A wildtype and mutant advanced CCOC. P values from generalized linear model with qausi-binomial distribution with values significant at the 0.05 level indicated in red.

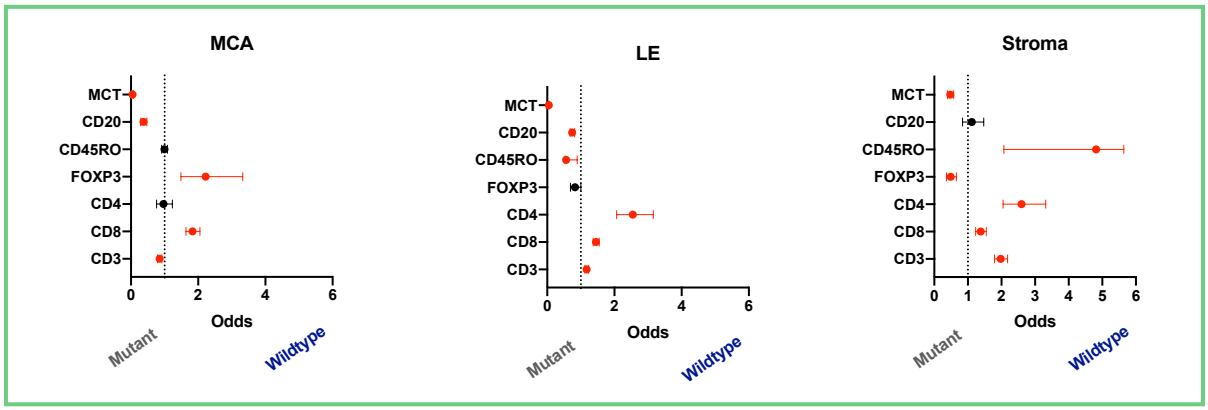


***Figure 1.22 Difference in immune cell markers quantified by positive cells per high power field, between ARID1A wildtype and mutant advanced clear cell ovarian cancers***

For immune markers quantified by positive cells per high power field, comparisons between ARID1A wildtype and mutant were made with chi-square with Yates correction and odds ratio plotted above; significant results shown in red.

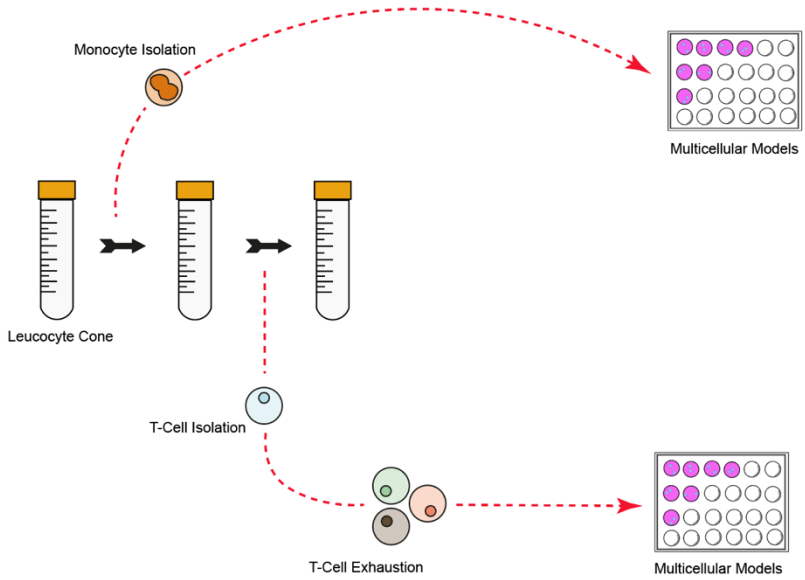


***Figure 1.24 Isolation of monocytes and T-cells from leucocyte cone for use in multicellular models***
Monocytes were initially isolated from the leucocyte cone using magnetic beads through a process of positive selection. Following this, naïve T cells were isolated via negative selection before undergoing an exhaustion protocol

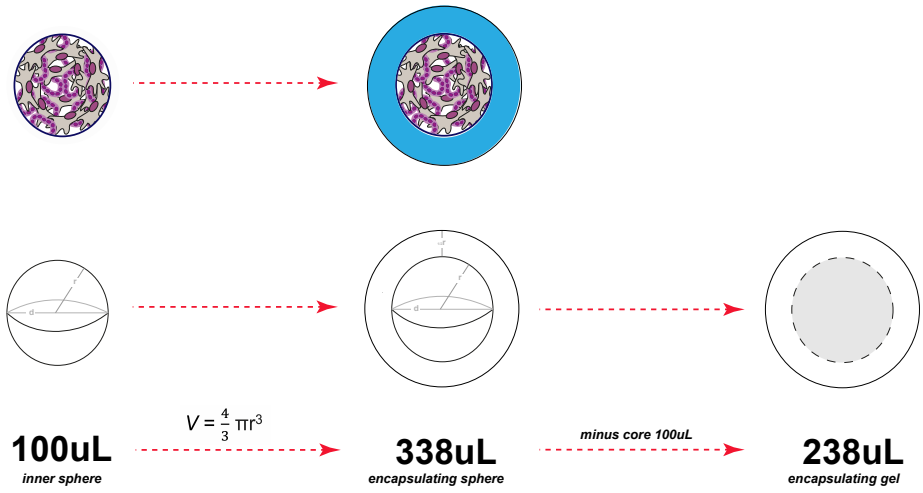


***Figure 1.25 Creation of the new encapsulated model of clear cell ovarian cancer***
To better recapitulate the tumour microenvironment of clear cell ovarian cancer, I cultured a malignant core with fibroblasts and immune cells for seven days before encapsulating this within another gel containing fibroblasts and immune cells. The volume of the malignant core was 100uL and for the encapsulating gel, 238uL. The collagen matrix to cellular component followed a 40:60 ratio; 1:1:2:1.5 ratios were used for malignant cells:fibroblasts:monocytes:Tcells based on ratios taken from CIBERSORT analysis of advanced CCOC.

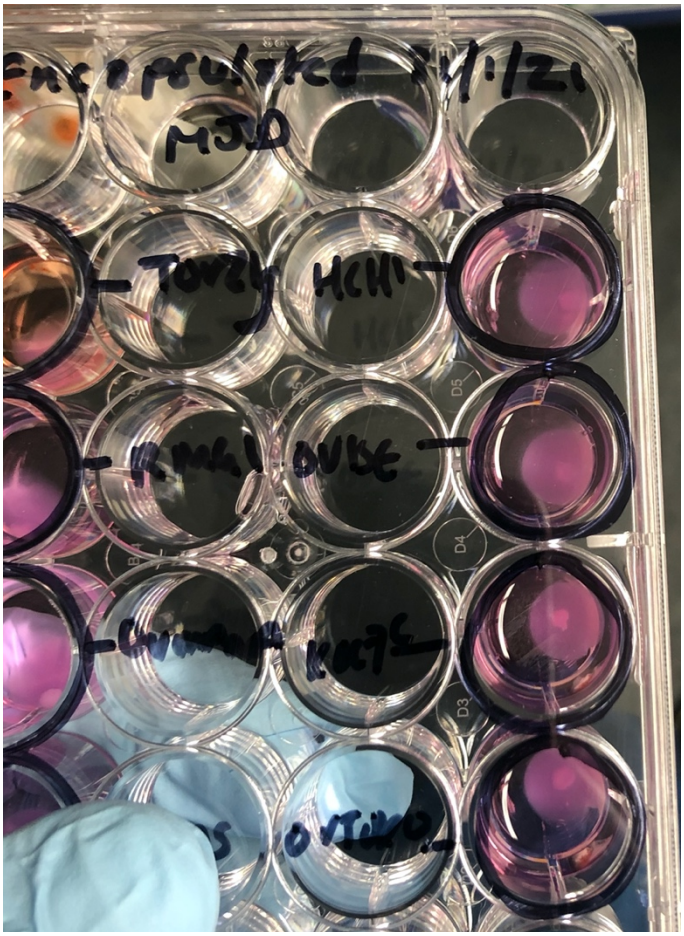

***Figure 1.26 Encapsulated mode of advanced clear cell ovarian cancer***
This shows a malignant core containing malignant cells, fibroblasts, monocytes and T cells within an outer gel of fibroblasts and immune cells. Once encapsulated, this model is viable for fourteen days.

***List of Publications and Presentations Resulting from the Translational Research Project "***The immune microenvironment of a murine model of clear cell ovarian cancer***"***

Abstracts

Devlin MJ, Kristeleit RS, McDermott J, Maniati E, Laforêts F, Kotantaki P, Miller RE, Balkwill F. Impact of ARID1A mutation on the tumour microenvironment of advanced clear cell ovarian cancer. AACR 2021 (accepted)

Devlin MJ, Kristeleit RS, McDermott J, Maniati E, Laforêts F, Kotantaki P, Miller RE, Balkwill F. The tumour microenvironment of advanced clear cell ovarian cancer. ESMO 2021 (planned submission)

Devlin MJ, Kristeleit RS, McDermott J, Maniati E, Laforêts F, Kotantaki P, Miller RE, Balkwill F. Impact of collagen thickness on the tumour microenvironment of advanced clear cell ovarian cancer. ESMO 2021 (planned submission)

Devlin MJ, Kristeleit RS, McDermott J, Maniati E, Laforêts F, Kotantaki P, Miller RE, Balkwill F. The evolution of the tumour microenvironment of clear cell ovarian cancer. ESMO 2021 (planned submission).

***List of Publications and Presentations resulting from other projects during the fellowship period (if***

***applicable)***

"The tumour microenvironment of advanced clear cell ovarian cancer" – manuscript in preparation.

***Selection of Courses and Workshops Attended During the Fellowship***

ESMO Congress
Beyond the Horizon: Innovative Cancer Drug Discovery
In Vitro 3D workshop
Opportunities in Ovarian Cancer
HHMT: ovarian cancer action
AACR

***Acknowledgements***

I would like to thank ESMO for affording me the opportunity to undertake research in an area that I feel very passionate about. This fellowship has allowed me to gain vital scientific skills and cultivate collaborations, both nationally and internationally, that I will continue to build on as I move forward with my career as a clinician scientist.

I am grateful to Professor Fran Balkwill and the entire Tumour Microenvironment group at Barts Cancer Institute for their support and guidance throughout the fellowship. Their dedication to improving patient outcomes through meaningful research continues to inspire me.

I would like to thank Professor David Bowtell (Peter MacCallum Cancer Centre, Australia) for granting access to RNA sequencing data and to Professor Chris Lord (Institute of Cancer Resarch, UK) for his gift of cell lines. I would also like to thank the Northern Ireland Biobank and the biobanks at University College London and Queen Mary University for their assistance in sample collection.

Finally, I would like to thank all the patients and their families for allowing samples to be used in this research project. Without their selfless contribution this project could not have happened.

***References***

**1.** Matz M, Coleman MP, Sant M, Chirlaque MD, Visser O, Gore M *et al. The histology of ovarian cancer: worldwide distribution and implications for international survival comparisons (CONCORD-2)*. *Gynecol Oncol* 2017; **144**: 405–413

**2.** Coburn SB, Bray F, Sherman ME, Trabert B. International patterns and trends in ovarian cancer incidence, overall and by histologic subtype. *Int J cancer* 2017; **140**: 2451–2460

**3.** Yamagami W, Nagase S, Takahashi F, Ino K, Hachisuga T, Aoki D *et al.* Clinical statistics of gynecologic cancers in Japan. *J Gynecol Oncol* 2017; **28**: e32

**4.** Machida H, Matsuo K, Yamagami W, Ebina Y, Kobayashi Y, Tabata T *et al.* Trends and characteristics of epithelial ovarian cancer in Japan between 2002 and 2015: A JSGO-JSOG joint study. *Gynecol Oncol* 2019; **153**: 589–596

**5.** Ho C-M, Huang Y-J, Chen T-C, Huang S-H, Liu F-S, Chang Chien C-C *et al.* Pure-type clear cell carcinoma of the ovary as a distinct histological type and improved survival in patients treated with paclitaxel-platinum-based chemotherapy in pure-type advanced disease. *Gynecol Oncol* 2004; **94**: 197–203

**6.** Takano M, Sugiyama T, Yaegashi N, Sakuma M, Suzuki M, Saga Y *et al.* Low response rate of second-line chemotherapy for recurrent or refractory clear cell carcinoma of the ovary: a retrospective Japan Clear Cell Carcinoma Study. *Int J Gynecol Cancer*; **18**: 937–42

**7.** Crotzer DR, Sun CC, Coleman RL, Wolf JK, Levenback CF, Gershenson DM. Lack of effective systemic therapy for recurrent clear cell carcinoma of the ovary. *Gynecol Oncol* 2007; **105**: 404–8

8. Matulonis UA, Shapira-Frommer R, Santin AD, Lisyanskaya AS, Pignata S, Vergote I *et al.* Antitumor activity and safety of pembrolizumab in patients with advanced recurrent ovarian cancer: results from the phase II KEYNOTE-100 study. *Ann Oncol Off J Eur Soc Med Oncol* 2019; **30**: 1080–1087

9. Bellone S, Buza N, Choi J, Zammataro L, Gay L, Elvin J *et al.* Exceptional response to pembrolizumab in a metastatic, chemotherapy/radiation-resistant ovarian cancer patient harboring a pd-l1-genetic rearrangement. *Clin Cancer Res* 2018. doi:10.1158/1078-0432.CCR-17-1805

10. Hamanishi J, Mandai M, Ikeda T, Minami M, Kawaguchi A, Murayama T *et al.* Safety and antitumor activity of Anti-PD-1 antibody, nivolumab, in patients with platinum-resistant ovarian cancer. *J Clin Oncol* 2015. doi:10.1200/JCO.2015.62.3397

11. Disis ML, Patel MR, Pant S, Infante JR, Lockhart AC, Kelly K *et al.* Avelumab (MSB0010718C), an anti-PD-L1 antibody, in patients with previously treated, recurrent or refractory ovarian cancer: A phase Ib, open-label expansion trial. *J Clin Oncol* 2015. doi:10.1200/jco.2015.33.15_suppl.5509

12. St Pierre R, Kadoch C. Mammalian SWI/SNF complexes in cancer: emerging therapeutic opportunities. *Curr Opin Genet Dev* 2017; **42**: 56–67

13. Wiegand KC, Shah SP, Al-Agha OM, Zhao Y, Tse K, Zeng T *et al.* ARID1A mutations in endometriosis-associated ovarian carcinomas. *N Engl J Med* 2010. doi:10.1056/NEJMoa1008433

14. Jones S, Wang TL, Shih IM, Mao TL, Nakayama K, Roden R *et al.* Frequent mutations of chromatin remodeling gene ARID1A in ovarian clear cell carcinoma. *Science (80- )* 2010. doi:10.1126/science.1196333

15. Shen J, Ju Z, Zhao W, Wang L, Peng Y, Ge Z *et al.* ARID1A deficiency promotes mutability and potentiates therapeutic antitumor immunity unleashed by immune checkpoint blockade. *Nat Med* 2018. doi:10.1038/s41591-018-0012-z.

16. Fukumoto T, Fatkhutdinov N, Zundell JA, Tcyganov EN, Nacarelli T, Karakashev S *et al.* HDAC6 Inhibition Synergizes with Anti-PD-L1 Therapy in ARID1A-Inactivated Ovarian Cancer. *Cancer Res* 2019; **79**: 5482–5489

17. Kawabata A, Yanaihara N, Nagata C, Saito M, Noguchi D, Takenaka M *et al.* Prognostic impact of interleukin-6 expression in stage I ovarian clear cell carcinoma. *Gynecol Oncol* 2017; **146**: 609–614

18. Kim M, Lu F, Zhang Y. Loss of HDAC-Mediated Repression and Gain of NF-κB Activation Underlie Cytokine Induction in ARID1A- and PIK3CA-Mutation-Driven Ovarian Cancer. *Cell Rep* 2016; **17**: 275–288

19. Chandler RL, Damrauer JS, Raab JR, Schisler JC, Wilkerson MD, Didion JP *et al.* Coexistent ARID1A-PIK3CA mutations promote ovarian clear-cell tumorigenesis through pro-tumorigenic inflammatory cytokine signalling. *Nat Commun* 2015; **6**: 6118

| ***SIGNATURES*** | |
|---|---|
| ***Award Recipient full name*** | ***Signature and Date*** |
| Michael-John Devlin | |

| ***Research Mentor full name*** | ***Signature and Date*** |
|---|---|
| Frances R Balkwill | |

**This ESMO Translational Fellowship Research Project was supported by an educational grant from Roche**